Dynamics of Free Carrier Absorption and Refractive Index Dispersion in Si and Si/PolySi Microrings

Marco Novarese, Sebastian Romero-Garcia, Jock Bovington, *Member, IEEE*, and Mariangela Gioannini, *Member, IEEE*

***Abstract*— We report pump-probe measurements of time resolved optical transmission spectra of Si and Si/poly-Si microrings after high free carrier densities have been generated by two-photon absorption of the pump pulse. From measurements, we can extract the recovery dynamics of free carrier absorption, refractive index dispersion, generated free carriers and finally the effective initial free carrier lifetimes. The method is validated by comparing modelling and simulations with measurements; the obtained results are in very good agreement with what predicted by the Shockley-Read-Hall recombination model for trap assisted recombination. We also propose a method for determining the empirical relations for free carrier absorption and refractive index dispersion in poly-Si waveguides.**

***Index Terms*— Silicon microrings, two-photon absorption, free carriers, polysilicon waveguide, carrier lifetimes.**

I. Introduction

SILICON microring resonators (MRRs) are important components in photonics integrated circuits due to their low-cost, low-power, and small-size properties achievable with CMOS fabrication processes [1]. One of the main drawbacks of using silicon at optical communication wavelengths is that Two-photon absorption (TPA), free carrier absorption (FCA), and dispersion (FCD) pose limitations to the power entering the MRR [2]. This problem is of great importance when employing microrings for hybrid tunable lasers based on the Vernier effect [3]. In order to reach wide tunability, a large free-spectral-range (FSR) is desired, which requires small ring radii. With silicon, it is possible to reach a ring radius of $r \approx 4\mu m$ with negligible bend loss. The ring radius can be further reduced to $2\mu m$ with only $5dB/cm$ of bend losses in the C band employing waveguide structures composed of Si and poly-Si core as those available in the SISCAP platform [4]. As discussed in the following of this letter, the waveguide consists in a rectangular undoped poly-Si core on top of a Si core. In poly-Si, the defects within the crystalline grains act as recombination centers for free carriers, dramatically decreasing the free carriers lifetimes with consequent reduced impact of FCA and increase of switching time when the MRR is employed as an all optical switch [5]. Free carrier lifetime is indeed a key parameter regulating the effective loss and the shift of the ring resonant wavelength. It is determined by trap-assisted non-radiative Shockley-Read-Hall (SRH) recombination [6] and thus by the density of holes in the valence band and of electrons in the conduction band [2]. Unfortunately, given the same electron and hole density in the Si and poly-Si core, the FCA in polysilicon is higher compared to crystalline silicon [7] since the FCA scales, as a first approximation, as $1/\mu_{n,p}$ [8] (with $\mu_{n,p}$ the carrier mobility) and the mobility in poly-Si is lower depending on the grain size and the number of grain boundaries that populate the material [9]. The aim of this letter is investigating the recovery of the free carriers (FC) via SRH recombination in crystalline Si and poly-Si waveguides, derive the corresponding lifetimes and, for the case of the poly-Si, the expressions for FCA and FCD as function of the free carrier density. To reach this goal, we have developed a method based on pump-probe experiments: we first retrieve the time resolved transmission spectra of the MRR as it recovers to the linear state after a strong pump pulse has excited the non-linearity. Then the nonlinear (NL) loss and the refractive index variation due to FC can be extracted, making it possible to experimentally determine the free carrier density inside the ring. With this approach, the carrier lifetimes in both structures can be retrieved demonstrating that in poly-Si they are one order of magnitude smaller than in Si waveguides. We validate our procedure by comparing the experimental results with ad hoc simulations, including trap-assisted recombination [2].

Manuscript received 13 December 2022; revised 17 February 2023; accepted 7 March 2023. Date of publication 10 March 2023; date of current version 16 March 2023. This work was supported in part by the European Union under the Italian National Recovery and Resilience Plan (NRRP) of NextGenerationEU, partnership on "Telecommunications of the Future," Program "RESTART," under Grant PE00000001. *(Corresponding author: Marco Novarese.)*

Marco Novarese and Mariangela Gioannini are with the Department of Electronics and Telecommunications (DET), Politecnico di Torino, 10129 Turin, Italy (e-mail: marco.novarese@polito.it; mariangela.gioannini@polito.it).

Sebastian Romero-Garcia and Jock Bovington are with Cisco Optical GmbH, 90411 Nuremberg, Germany (e-mail: sromerog@cisco.com; jbovingt@cisco.com).

Color versions of one or more figures in this letter are available at https://doi.org/10.1109/LPT.2023.3255299.

Digital Object Identifier 10.1109/LPT.2023.3255299

II. Experimental Setup

Fig.1 shows the setup for continuous wave (CW) or pump-probe characterization of the MRRs. We inject a pump pulse of 100 ps with different pump energies and wavelength set at one of the resonant wavelengths ($\lambda_{0,pump}$) of the microring in linear regime. The CW probe power in the bus is below $-20\,dBm$. To measure the impact of NL effects on the transmission coefficient of the ring, the probe wavelength (λ_{probe}) is varied around a resonant wavelength ($\lambda_{0,probe}$) whereas the pump wavelength is fixed at the closest resonant wavelength of the ring ($\lambda_{0,pump}$, on the red side with respect to $\lambda_{0,probe}$, see the inset of Fig. 1).

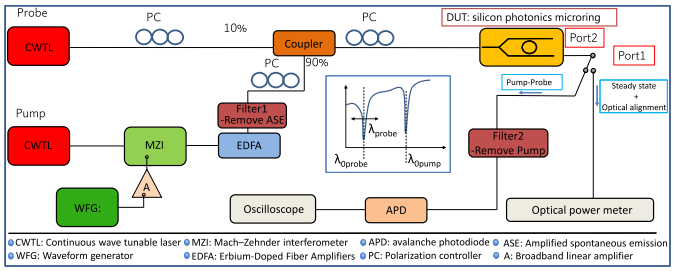

Fig. 1. Setup implemented in CW and pump-probe MRR measurements.

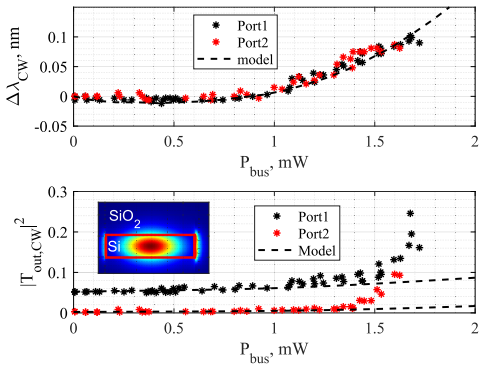

Fig. 2. Measured and modelled variation of the resonant wavelength and transmission coefficients for CW power injection. Ring with rectangular waveguide cross section and radius $r = 5\,\mu m$. From fitting we get $N_t = 8.5 \cdot 10^{16}\,cm^{-3}$.

Once the pump pulse has been absorbed due to TPA and the free electrons and holes have been generated, the CW probe at different wavelengths monitors in time the nonlinear response of the ring as a result of FCA and FCD.

Since the pump repetition rate ($4\,kHz$) is much larger than the pump pulse, we avoid any thermal effects. To understand the experimental results, we employ the model we developed in [2] to simulate the CW nonlinear response of silicon MRR. The model in [2] can be extended to the time domain [10] to simulate the nonlinear response of the ring after the pump pulse. FC recombination is modeled by trap-assisted Shockley-Read-Hall (SRH) rate equations [2]. The density of trap (N_t) in the Si core determines the SRH recombination rate of electrons and holes and it is the free parameter to fit the experiments.

III. Results

We have first characterized a Si MRR with CW input power and forward wavelength sweep to retrieve from modelling and fitting the trap density per unit of volume N_t and other linear parameters [2]. The cross section of the MRR waveguide is in the inset of Fig.2.

The measured and simulated variation of the ring resonant wavelength ($\Delta\lambda_{CW}$) and the transmission coefficients at the two output ports (through ports 1 and 2 in Fig. 1) at resonance ($T_{out,CW}$) are reported in Fig. 2; P_{bus} is the power entering the splitter (see the MRR structure of the device-under-test, DUT, in Fig. 1). The model [2] well reproduces the shift of resonant wavelength and transmission coefficient as function of the bus power. Discrepancy at power higher than $1.6\,mW$ are due to the self-oscillations of the ring [10]. To experimentally retrieve the recovery dynamics of the free carrier densities, we have performed pump-probe measurements; results are in Fig. 3. Fig. 3 (a) collects the respectively maps of the measured and simulated probe traces at different wavelengths with the pump pulse of $100\,ps$ injected at $5.1\,ns$ in the time axis. From the measured map in Fig. 3 (a) we construct in Fig. 3 (b) the measured spectrum of the transmission coefficients of the ring at different time instants after the pump has ended at $t = 5.4\,ns$. We observe the recovery of the ring transmission spectrum from the maximum of the nonlinear response (blue spectrum just after the pump) to the linear response (purple curve). By fitting, with the analytical expression of the transmission spectrum, the spectra measured at the different time instants, we can extract the variation with time of the optical modal loss ($\alpha(t)$) inside the ring and the loss variation, due to FCA, with respect to the linear value $\alpha_{0,tot}$; that is $\Delta\alpha_{FCA,exp}(t) = \alpha(t) - \alpha_{0,tot}$. Here $\alpha_{0,tot} = \alpha_0 + \alpha_{rad}$, where α_0 is the linear loss term due to light scattering, surface state absorption, and residual doping, while α_{rad} accounts for light irradiated in the cladding due to bend loss. TPA loss of the probe signal in the time range after the pump pulse are negligible because the circulating probe power is low. From the minima of the transmission spectra, we get the variation of the resonant wavelength ($\Delta\lambda_{exp}(t)$) with respect to the linear case and then the variation of the waveguide refractive index due to FCD: $\Delta n_{eff,FCD}(t) = \Delta\lambda(t) \cdot n_g/\lambda_0$ [8]. Here λ_0 is the cold resonance of the ring and $n_g = 3.45$ is the group index of the silicon waveguide. The results are in Fig. 3 (c), the black solid lines are the model results in good agreement with the experiments, where we attribute the small discrepancy in NL losses between measurements and model to the noise of the avalanche photodiode (APD) and additional insertion losses in the filter-APD-oscilloscope configuration. The variation of the silicon optical loss and refractive index depends on the density of electrons (n_e) and holes (p_e) as derived by Soref et al. [11], namely:

$$\Delta\alpha_{FCA} = \Gamma\left(8.88 \cdot 10^{-21} n_e^{1.167} + 5.84 \cdot 10^{-20} p_e^{1.109}\right), \tag{1}$$

$$\Delta n_{eff,FCD} = -\Gamma(5.4 \cdot 10^{-22} n_e^{1.011} + 1.53 \cdot 10^{-18} p_e^{0.838}). \tag{2}$$

where Γ is the optical confinement factor of the field in the silicon core. Having measured in Fig.3 (b) these variations, we can compute numerically from eqs.(1) and (2) the electron and hole densities with the constraint $0 < (p_e - n_e)/N_t < 1$; $(p_e - n_e)/N_t$ is the fraction of occupied traps [2], [6], [10]. Results are displayed in Fig.4; the difference between electron and hole densities is justified by the different capture times in the trap for electrons and holes. By fitting the curve with a single exponential, we can extract the initial electron and hole equivalent lifetimes referred to the first $10\,ns$ of carrier transient [12]. These are summarized in Table I. We note that the electron lifetime decreases with increasing power while the hole lifetime follows the opposite trend; this is well explained by the SRH theory, where the nonlinear behavior of both carriers is determined by the trap density and trap energy level [2], [6], [10]. The model we developed in [2] and [10] is also fairly accurate in following the experimental results with

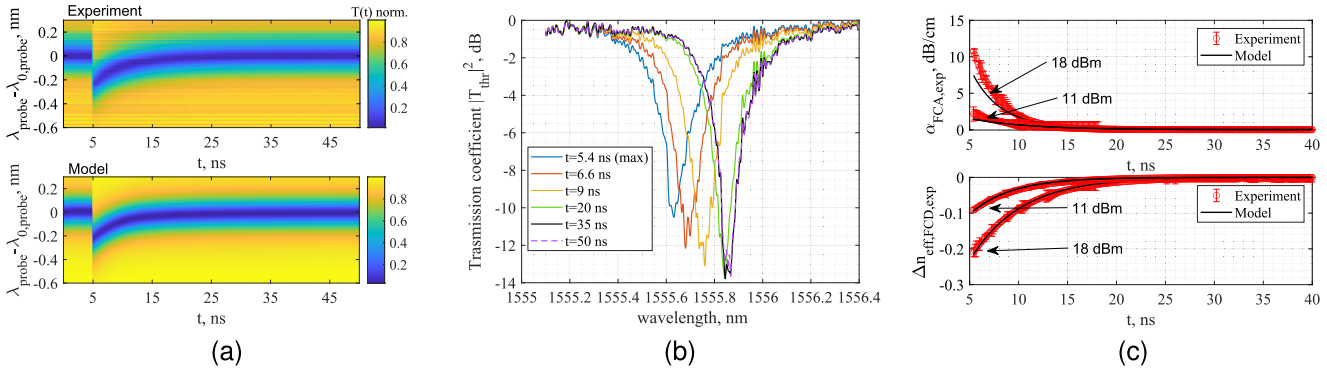

Fig. 3. (a) Measured c-Si waveguide (top) and simulated (bottom) probe traces at different wavelengths in the case of a pump pulse of 100 ps injected at 5.1 ns and peak power of 18 dBm. (b) Transmission spectrum of the ring reconstructed from Fig. 3 (a) at different time instants after the pump at $t = 5.4\,ns$. (c) Extracted variation of nonlinear losses and resonant wavelength due to FCA and FCD for two different pulse peak power.

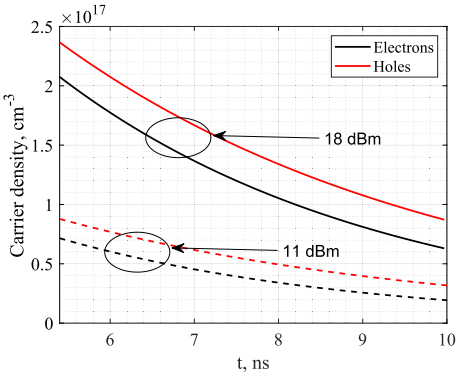

Fig. 4. Electron and hole carrier densities versus time extracted by the measured traces in Fig.3 (c).

TABLE I
EXPERIMENTAL AND SIMULATED INITIAL ELECTRON AND HOLE LIFETIMES

$\tau[ns]$	Experiment	Theory
$\tau_{n,18dBm}$	3.6	2.7
$\tau_{p,18dBm}$	4.35	5
$\tau_{n,11dBm}$	1.15	0.83
$\tau_{p,11dBm}$	6.5	6.4

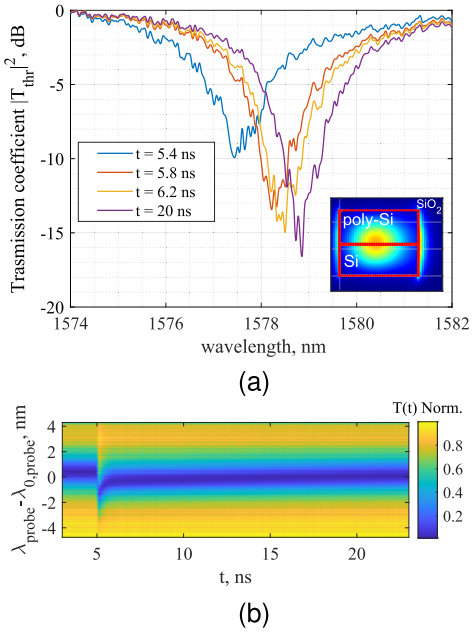

Fig. 5. (a) Time-resolved transmission spectra of the Si/poly-Si ring and related probe trace (b). The inset in (a) shows a schematic cross-sectional view of the ring. A pump pulse of 100 ps is injected at 5.1 ns with peak power of $P_{bus,peak} \approx 24\,dBm$.

the carrier lifetimes being close to the experimental values. The good match between the model and experimental results also validates the experimental procedure we have set up. The approach developed in the standard silicon MRR case has been extended to the characterization of the Si/poly-Si MRR, whose cross section is shown in the inset of Fig.5 (a). In the pump-probe experiments, the pulse width and period are the same as in the previous case, whereas a higher pump peak power of approximately 24dBm has been injected to excite enough free carries in both Si and poly-Si cores. Time-resolved transmission spectra (Fig.5(a)) are recovered from the map of measured probe traces (in Fig.5 (b)) after the pump pulse of 100 ps has ended at 5.4 ns. The extracted variation of loss $\Delta\alpha_{FCA,exp}(t)$ and the effective refractive index $\Delta n_{eff,FCD,exp}(t)$ are in Fig.6 in black solid line. To obtain information about the carrier density inside the Si and poly-Si cores, we fit the measured recovery with a double exponential function: the fastest decaying exponential (blue curves in Fig.6) is associated with poly-Si [13], whereas the other one (dashed red line in Fig.6) is related to silicon. In fact the optical field is almost equally confined in both cores ($\Gamma_{Si} = 0.46$ and $\Gamma_{poly} = 0.51$). Assuming that β_{TPA} is equal in both materials, we expect approximately the same number of carriers (generated by TPA) in the Si and poly-Si cores immediately after the pump at $t = 5.4\,ns$ (i.e., $n_{e,Si}(t = 5.4\,ns) = n_{e,poly-Si}(t = 5.4\,ns)$ and $p_{e,Si}(t = 5.4\,ns) = p_{e,poly-Si}(t = 5.4\,ns)$). We can use then Eq.(1) and (2) to fit the red dashed curves of the silicon response and retrieve the carrier density in silicon. The values of carrier density calculated in Si at $t = 5.4\,ns$, are employed to find, from the blue curves at $t = 5.4\,ns$, the coefficients A_{poly}, B_{poly}, C_{poly}, D_{poly} of the expressions:

$$\Delta\alpha_{FCA,poly} = \Gamma_{poly}\left(A_{poly}n_e^{1.167} + B_{poly}p_e^{1.109}\right), \quad (3)$$

$$\Delta n_{eff,FCD,poly} = -\Gamma_{poly}(C_{poly}n_e^{1.011} + D_{poly}p_e^{0.838}). \quad (4)$$

The minimization procedure results in the values $A_{poly} = 5.2 \cdot 10^{-20}\,cm^2$,$B_{poly} = 1.2 \cdot 10^{-19}\,cm^2$,$C_{poly} = 6.6 \cdot 10^{-22}\,cm^3$, and $D_{poly} = 2.4 \cdot 10^{-18}\,cm^3$. We note that the coefficients A_{poly} and B_{poly} are one order of magnitude higher than

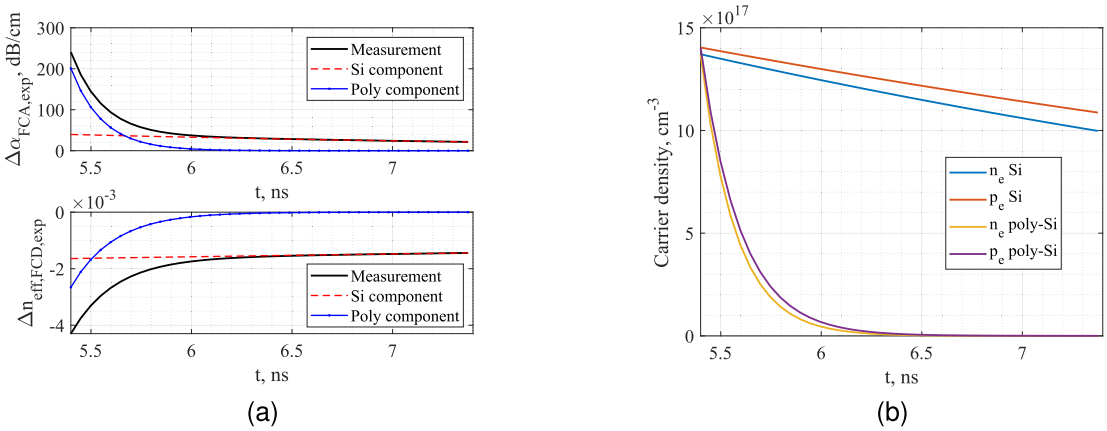

Fig. 6. (a) Losses and refractive index variation in the Si/poly-Si ring recovered from the pump and probe traces with two exponential functions (blue line attributed to FC recovery in poly-Si) and dashed red line (attributed to FC recovery in Si); (b) Resulting electron and hole carrier densities in the Si and poly-Si cores.

TABLE II
EXPERIMENTAL INITIAL CARRIER LIFETIMES IN SI/POLY-SI WAVEGUIDES

$\tau[ns]$	Silicon	polysilicon
τ_n	6.4	0.17
τ_p	7.7	0.2

those of silicon, which means that poly-Si suffers a higher FCA as expected by the reduced carrier mobility [8]. Fixing the previous coefficients and from Eq.(1)-(4), we can get the carrier densities with time as reported in Fig.6 (b); the extracted initial carrier lifetimes are summarized in Table II.

IV. CONCLUSION

We have presented pump-probe experiments to retrieve the time resolved transmission spectra in nonlinear regime in Si microring resonators excited by strong pump pulses. The analysis of the measured spectra allows the extraction of the absorption and refractive index variation in time. From these two quantities, we have recovered the dynamics of free electrons and holes and their equivalent initial lifetimes in two types of resonators. Simulation results obtained with a time domain nonlinear model of the rings, including SRH trap-assisted recombination, were able to fit the experimental data for the silicon waveguide, allowing the material properties of the tested waveguides to be quantified using the developed experimental methodology.

ACKNOWLEDGMENT

The authors acknowledge Prof. Ronqui Hui, University of Kansas. for the collaboration in the initial part of this work.

REFERENCES

[1] W. Bogaerts et al., "Silicon microring resonators," *Laser Photon. Rev.*, vol. 6, no. 1, pp. 47–73, 2012.
[2] M. Novarese, S. R. Garcia, S. Cucco, D. Adams, J. Bovington, and M. Gioannini, "Study of nonlinear effects and self-heating in a silicon microring resonator including a Shockley-Read-Hall model for carrier recombination," *Opt. Exp.*, vol. 30, no. 9, p. 14341, Apr. 2022.
[3] L. Columbo, J. Bovington, S. Romero-Garcia, D. F. Siriani, and M. Gioannini, "Efficient and optical feedback tolerant hybrid laser design for silicon photonics applications," *IEEE J. Sel. Topics Quantum Electron.*, vol. 26, no. 2, pp. 1–10, Mar. 2020.
[4] M. Webster et al., "An efficient MOS-capacitor based silicon modulator and CMOS drivers for optical transmitters," in *Proc. 11th Int. Conf. Group IV Photon. (GFP)*, Aug. 2014, pp. 1–2.
[5] C. Manolatou and M. Lipson, "All-optical silicon modulators based on carrier injection by two-photon absorption," *J. Lightw. Technol.*, vol. 24, no. 3, pp. 1433–1439, Mar. 2006.
[6] D. K. Schroder, "Carrier lifetimes in silicon," *IEEE Trans. Electron Devices*, vol. 44, no. 1, pp. 160–170, Jan. 1997.
[7] A. V. Shah et al., "Material and solar cell research in microcrystalline silicon," *Sol. Energy Mater. Sol. Cells*, vol. 78, nos. 1–4, pp. 469–491, 2003.
[8] Q. Lin, O. J. Painter, and G. P. Agrawal, "Nonlinear optical phenomena in silicon waveguides: Modeling and applications," *Opt. Exp.*, vol. 15, no. 25, pp. 16604–16644, Dec. 2007.
[9] J. Martinez and J. Piqueras, "On the mobility of polycrystalline semiconductors," *Solid-State Electron.*, vol. 23, no. 4, pp. 297–303, 1980.
[10] M. Novarese, S. Romero Garcia, S. Cucco, D. Adams, J. Bovington, and M. Gioannini, "Study of nonlinear effects and self-heating in silicon microring resonator including SRH model for carrier recombination," *Proc. SPIE*, vol. 12006, Mar. 2022, Art. no. 120060G.
[11] M. Nedeljkovic, R. Soref, and G. Z. Mashanovich, "Free-carrier electrorefraction and electroabsorption modulation predictions for silicon over the 1–14-μm infrared wavelength range," *IEEE Photon. J.*, vol. 3, no. 6, pp. 1171–1180, Dec. 2011.
[12] I. Aldaya, A. Gil-Molina, J. L. Pita, L. H. Gabrielli, H. L. Fragnito, and P. Dainese, "Nonlinear carrier dynamics in silicon nano-waveguides," *Optica*, vol. 4, no. 10, pp. 1219–1227, 2017.
[13] J. S. Pelc, K. Rivoire, S. Vo, C. M. Santori, D. A. Fattal, and R. G. Beausoleil, "Picosecond all-optical switching in hydrogenated amorphous silicon microring resonators," *Opt. Exp.*, vol. 22, no. 4, pp. 3797–3810, 2014.

Open Access funding provided by 'Politecnico di Torino' within the CRUI CARE Agreement